



Methods for the Automated Determination of Sustained Maximum Amplitudes in Oscillating Signals

Nathaniel DeVol

George W. Woodruff School of Mechanical Engineering,
Georgia Institute of Technology,
801 Ferst Drive,
Atlanta, GA 30332
e-mail: ndevol3@gatech.edu

Christopher Saldaña

George W. Woodruff School of Mechanical Engineering,
Georgia Institute of Technology,
801 Ferst Drive,
Atlanta, GA 30332
e-mail: christopher.saldana@me.gatech.edu

Katherine Fu¹

Department of Mechanical Engineering,
University of Wisconsin-Madison,
1513 University Avenue,
Madison, WI 53706
e-mail: kate.fu@wisc.edu

Machine condition monitoring has been proven to reduce machine downtime and increase productivity. The state-of-the-art research uses vibration monitoring for tasks such as maintenance and tool wear prediction. A less explored aspect is how vibration monitoring might be used to monitor equipment sensitive to vibration. In a manufacturing environment, one example of where this might be needed is in monitoring the vibration of optical linear encoders used in high-precision machine tools and coordinate measuring machines. Monitoring the vibration of sensitive equipment presents a unique case for vibration monitoring because an accurate calculation of the maximum sustained vibration is needed, as opposed to extracting trends from the data. To do this, techniques for determining sustained peaks in vibration signals are needed. This work fills this gap by formalizing and testing methods for determining sustained vibration amplitudes. The methods are tested on simulated signals based on experimental data. Results show that processing the signal directly with the novel Expire Timer method produces the smallest amounts of error on average under various test conditions. Additionally, this method can operate in real-time on streaming vibration data. [DOI: 10.1115/1.4063130]

Keywords: data-driven engineering, Industrial Internet of Things

¹Corresponding author.

Manuscript received October 19, 2022; final manuscript received August 4, 2023; published online August 25, 2023. Assoc. Editor: Yan Lu.

1 Introduction

With rising environmental concerns, there is an increased need for sustainable manufacturing with respect to maintenance programs and resource efficiency [1]. The recent rise in the Internet of Things (IoT) [2] and the Industrial Internet of Things (IIoT) [3] have helped to address these needs by providing insights into manufacturing processes. The ability of manufacturing systems to communicate allows for predictive and prescriptive operations that can improve performance and realize invisible issues [4]. The most common maintenance program that uses the IIoT is condition-based maintenance. Condition-based maintenance uses condition monitoring of a machine to predict when a machine will require maintenance [5]. While part quality and machine condition are traditionally studied separately, it is clear they are strongly interrelated [6]. In precision manufacturing, one example of where these two areas merge is in the machine's encoders.

A prior survey found that optical encoders account for the majority of sensors used for precision positioning [7]. Optical encoders are comprised of a reader head and a scale that can be either linear or rotary. The scale has graduations that the reader head uses to measure displacement [8]. Errors from a machine's encoder are translated into errors in the part's dimensions so it is important to consider sources of error for encoders. One source of error for optical encoders is related to mechanical effects from deformations, temperature variation, or vibration [9]. Vibrations of optical linear encoders are important because when the scanning head is vibrating in relation to the scale, the vibration movement is registered as spindle movement resulting in positional error [10,11]. In extreme conditions, the vibrations can cause temporary or permanent loss of position [9]. These errors directly translate to dimensional errors in the parts being produced.

Encoder manufacturers specify acceptable vibration levels with two components: shock and sustained. The shock limit can be easily determined by checking for signal values that cross a threshold. The sustained limit, however, has a time associated with it for which an amplitude must persist before it is considered sustained. In this work, this time is referred to as $t_{\text{sustained}}$. Because vibration signals are oscillating, the sustained maximum of a signal cannot be determined by simply detecting if the incoming signal remains above the threshold for the specified time. Monitoring sustained peaks, or bursts, is of interest in other domains [12–21]. Previous methods are not suitable for monitoring vibration because they either do not work with oscillating signals or do not return any amplitude information. For these reasons, this work investigates the efficacy of methods for extracting the sustained maximums from vibration data for use in condition monitoring of optical encoders. The impact of noise levels with stationary and non-stationary signals is explored.

2 Material and Methods

For the motivating example, $t_{\text{sustained}}$ was set at 20 ms, since this is the specification set by the glass scale manufacturer, Heidenhain (Traunreut, Germany). All methods developed here can be extended to other applications with different $t_{\text{sustained}}$ values. Throughout the development of the methods in this section, two signals were used for demonstration purposes. Both signals consisted of a base signal with two Gaussian disturbances. The equations used to generate the base test signals are given in Eqs. (1) and (2). The base frequency of 70 Hz was chosen because it is the tooth pass frequency of the experimental data which the simulated data were based on. In

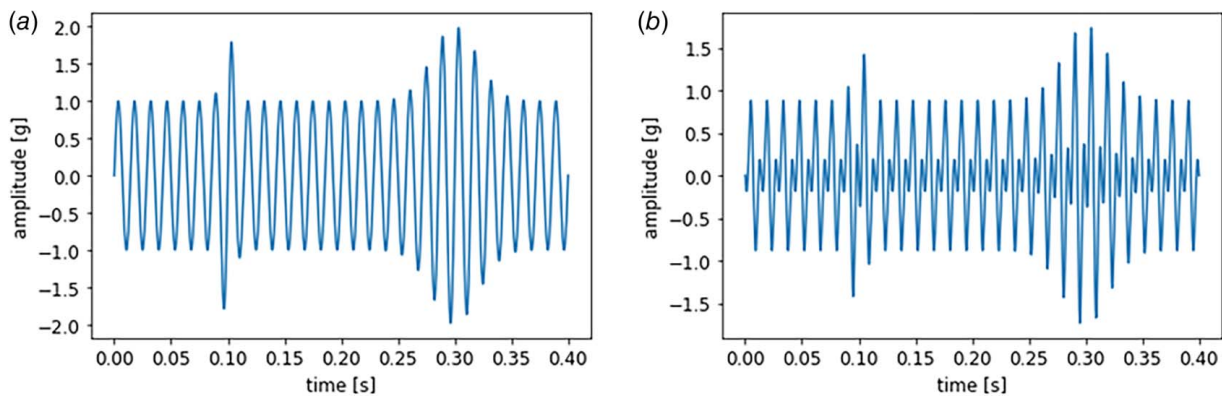


Fig. 1 Test signals used to demonstrate methods: (a) single sine function and (b) two sine functions

the second signal, a harmonic created by doubling the 70 Hz base frequency was added.

$$\text{signal 1} = \sin(70 * 2 * \pi * t) \quad (1)$$

$$\begin{aligned} \text{signal 2} = & \frac{1}{2} * \sin(70 * 2 * \pi * t) \\ & + \frac{1}{2} * \sin(140 * 2 * \pi * t + \pi) \end{aligned} \quad (2)$$

These equations were used to create a 0.4 s signal sampled at 10,000 Hz. Two Gaussian disturbances were then applied. A

narrow Gaussian disturbance with a standard deviation of 0.005 was applied at 0.1 s. A wide Gaussian disturbance with a standard deviation of 0.02 was applied at 0.3 s. The created signals are shown in Fig. 1.

2.1 Envelope-Based Methods. The first collection of methods forms an envelope around the signal and determines the maximum sustained amplitude from the envelope. Three envelop-based methods are developed and tested. These methods are referred to as the *Moving RMS*, short-time Fourier transform (*STFT*) *Peaks*, *Peak Envelope*, and *low pass (LP) Rectifier Envelope* methods. Once the signal is bound by one of these envelope methods, the sustained amplitudes are determined from the bounded signal as if it was non-oscillating. The process of doing this is detailed in Sec. 3.2.

The *Moving RMS* method first calculates the RMS of the signal over a sliding window. The amplitude (a) of the signal ($x(t)$) is then determined as $a = \text{RMS}(x(t)) * \sqrt{2}$. When applying the method, a window size must be properly selected. To determine the proper window size, a minimum frequency, f_{\min} , is specified. From Fig. 2, it was determined that the window size should be twice the period of f_{\min} so that the calculated RMS over the moving window is within 5% of the RMS of a signal of infinite length. An example of the RMS method, with a window size of 40 ms, applied to the two test signals is shown in Fig. 3. From these initial results, it appears that the moving RMS works well on the signal with a single frequency, but a large amount of error is present when the second frequency is introduced.

The next method, *STFT Peaks*, forms an envelope by summing the amplitudes of each peak in the Fourier transform of each time segment. One potential shortcoming of this method is that if many sinusoidal functions are present in the signal, the amplitude

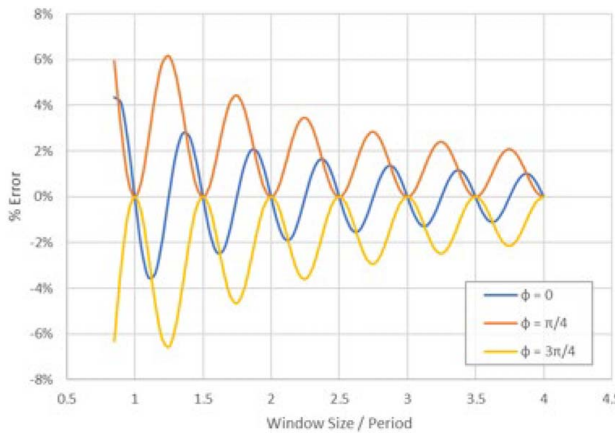


Fig. 2 The percentage error of the amplitude of a sine wave calculated from its RMS for different window sizes and phase angles

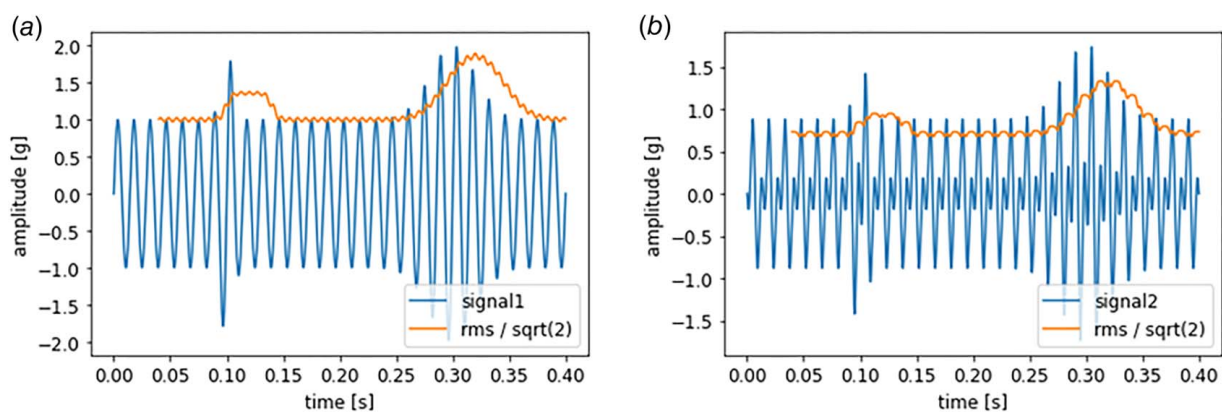


Fig. 3 Example implementation of the *Moving RMS* method bounding (a) a 70 Hz signal and (b) a composite 70 Hz and 140 Hz signal, both with two Gaussian disturbances

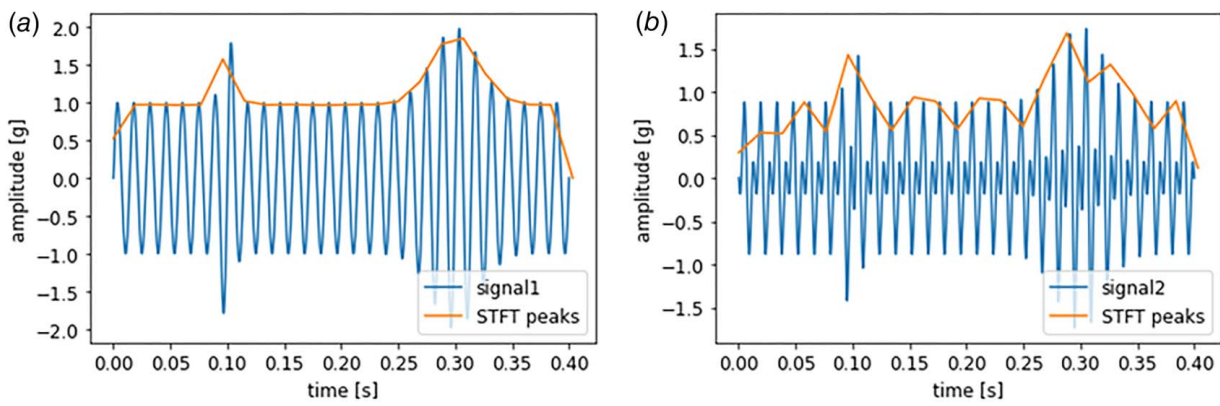


Fig. 4 Example implementation of STFT Peaks method bounding (a) a 70 Hz signal and (b) a composite 70 Hz and 140 Hz signal, both with two Gaussian disturbances

obtained by summing all the peaks in the Fourier transform may not be realized in the signal. When using the STFT, it is important to appropriately select values for the window and hop sizes as well as the window function itself. In this work, the Hann window was used because it attenuates boundary effects and offers compact support [22]. For the sample signals used in this section, a window size of 256 samples is used with a hop size of 64 samples. These sample signals are sampled at 10,000 Hz, so these STFT parameters will offer a resolution of 6.4 ms, which was sufficient for detecting sustained periods longer than 20 ms. The final parameter to select is the threshold which constitutes a real peak. Because noise will add small peaks to the Fourier transform, and peaks that are less than 10% of the highest peak are discarded. This STFT Peaks method was applied to the two samples from the beginning of this section, and the results are shown in Fig. 4.

The third method for determining the envelope of the signal, the *Peak Envelope* method, involves fitting a curve to the peaks in a signal. This method is used in the initial step of the empirical mode decomposition where a cubic spline is used to envelop the data [23]. In this work, the PYTHON package SciPy was used to find the maxima in the data by comparing neighboring values [24]. To avoid high-frequency noise, the local maxima are separated by at least $t_{\text{sustained}}/2$. Once the peaks are found, a univariate spline is fit to the local maxima. The result of applying this technique to the two test signals is shown in Fig. 5. For reference, the local maxima that the spline is fit to are shown in Fig. 5.

The last method that forms an envelope around the signal, the *LP Rectifier Envelope* method, is based on the bandwidth reduction approach used by Jeong et al. [25]. In its implementation in this work, the absolute value of the signal was used as the starting envelope. The results of applying this method to the two example signals

used in this section are shown in Fig. 6. It is important to note that the parameters of the bandwidth reduction must be carefully selected. For the examples presented here, the first LP filter had a cutoff of 10 Hz and order 5. The second low pass filter had a cutoff of 200 Hz and order 5. The process was completed twice to ensure that the envelope bounds the input signal.

2.2 Peak Height at Width. For the envelope-based methods, the maximum amplitude that persists for the critical threshold of $t_{\text{sustained}}$ is determined by iteratively calling SciPy's *peak_width* function [24]. The *peak_widths* function calculated the width of a peak at a specified relative height. The relative height used is updated and retested until the returned width is within 2% of $t_{\text{sustained}}$. If no peaks exist in the envelope signal, which corresponds to a signal with no disturbances, the average of the envelope will be returned as the maximum sustained amplitude.

2.3 Non-Envelope-Based Methods. In addition to the four methods that are based on forming an envelope around the signal and determining the maximum sustained amplitude from the envelope, two methods that work directly on the raw signal directly were developed and tested. These methods are referred to as the *Peak Distances* and *Expire Timer* methods.

In the absence of noise, and at a sufficient sampling rate, the distances between peaks can be used to find the maximum sustained amplitudes. To execute this method, the peaks must first be located. The list is then sorted according to descending amplitude and iterated through, beginning with the second list item (second highest peak). The time between the peak under investigation and all peaks higher on the list, which will have higher amplitudes

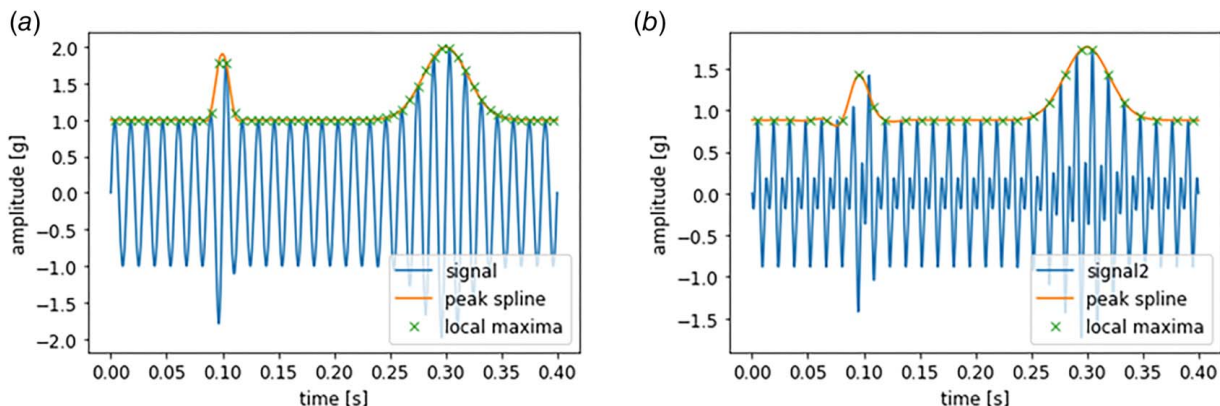


Fig. 5 Example implementation of Peak Envelope method bounding (a) a 70 Hz signal and (b) a composite 70 Hz and 140 Hz signal, both with two Gaussian disturbances

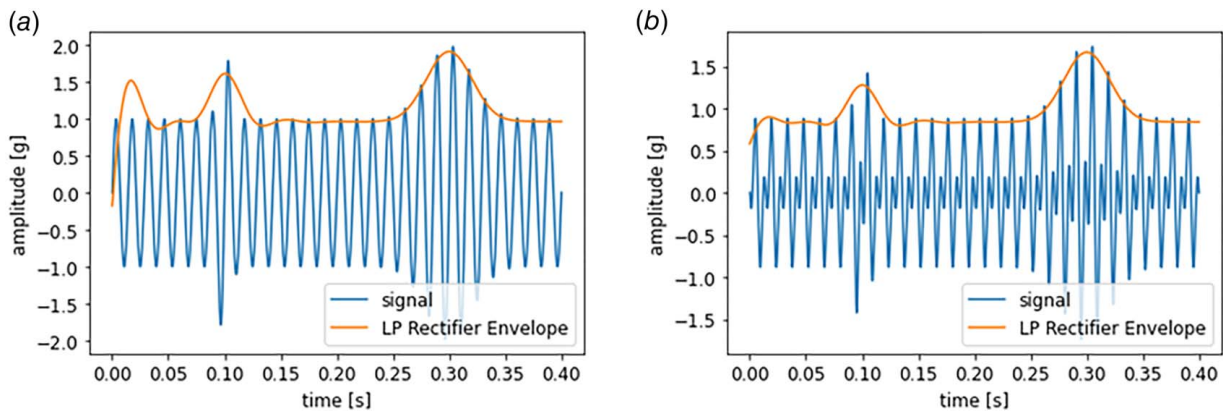


Fig. 6 Example implementation of LP Rectifier Envelope method bounding (a) a 70 Hz signal and (b) a composite 70 Hz and 140 Hz signal, both with two Gaussian disturbances

than the peak under investigation, are calculated. If the time is greater than $t_{sustained}$, then a sustained amplitude at the level of the peak under investigation is said to be present. This is the basis for the *Peak Distances* method.

One shortcoming of this method is that only two peaks need to be present, and this makes it susceptible to noise. It also does not account for multiple disturbances that may exist within a segment of signal under analysis. For example, when the same 70 Hz signal test signal with two Gaussian disturbances was applied here, the sustained amplitude was shown to span the two disturbances in Fig. 7(a), but the method was successful when a single disturbance is present as shown in Fig. 7(b). For lower sampling rates, it is also likely that peaks will be missed.

The final method, the *Expire Timer* method, resembles the *Peak Distances* method, but it incorporates an expire timer so that long gaps between two amplitudes will not be registered as a sustained amplitude. The length of the expire timer t_{expire} will be set by the desired minimum detectable frequency f_{min} . The t_{expire} must be at least the length of time between peaks in f_{min} . Because the absolute value of the signal is analyzed, two peaks will occur in each period, the relation between f_{min} and t_{expire} is given in Eq. (3).

$$t_{expire} = \frac{1}{2 * f_{min}} \quad (3)$$

Once the length of the expire timer is set, the maximum sustained amplitude is determined by storing two values: *lastSustained* which stores the highest amplitude that has been determined to reach the sustained time criteria, and *lastTooHigh*

which stores the lowest amplitude where that was considered not to be a sustained amplitude. The maximum of the signal is used to initialize *lastTooHigh* and *lastSustained* is initialized to zero. In each iteration, the average of *lastTooHigh* and *lastSustained* is tested. If it is determined to be a sustained amplitude, then *lastSustained* is updated. If not, *lastTooHigh* is updated. The process can continue until either a specified number of iterations are completed or until the change in the test value between iterations is below a threshold.

To determine if the amplitude under consideration is sustained or not, the test amplitude is used to threshold the rectified signal. From this thresholded signal, it is determined if the test amplitude is sustained or not by scanning each data point. If the value is zero, it moves to the next point. If the value is one, two timers are created. One timer is counting to determine if $t_{sustained}$ is reached and is referred to as the sustained timer. The second timer is counting to determine if t_{expire} is reached and is referred to as the expire timer. The expire timer is reset each time a value of one is seen. The sustained timer is reset only when the expire timer reaches its limit. The functions of these two timers are illustrated in Fig. 8. At the start of the first Gaussian disturbance, the sustained timer is started. For each nonzero value, the expire timer is reset as the signal is scanned. When the portion of the signal that no longer crosses the threshold is reached, the expire timer will run out, and the sustained timer will be reset. When the signal passes the threshold again at the start of the second disturbance, the sustained timer is reset. This time, the sustained timer is able to complete without the expire timer canceling it, so a sustained amplitude at the test amplitude of 1.1 g is determined to be present.

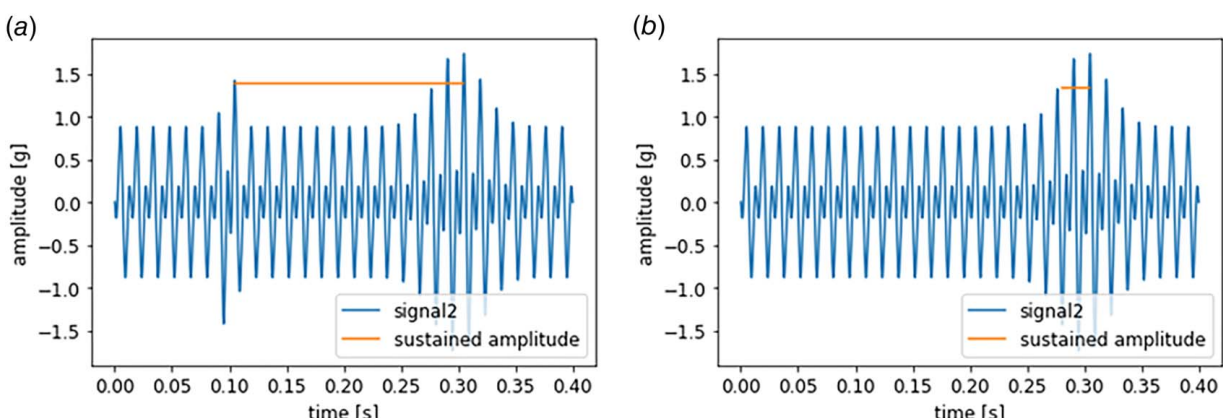


Fig. 7 Example implementation of Peak Distances method applied to a test signal with (a) two Gaussian disturbances and (b) a single Gaussian disturbance

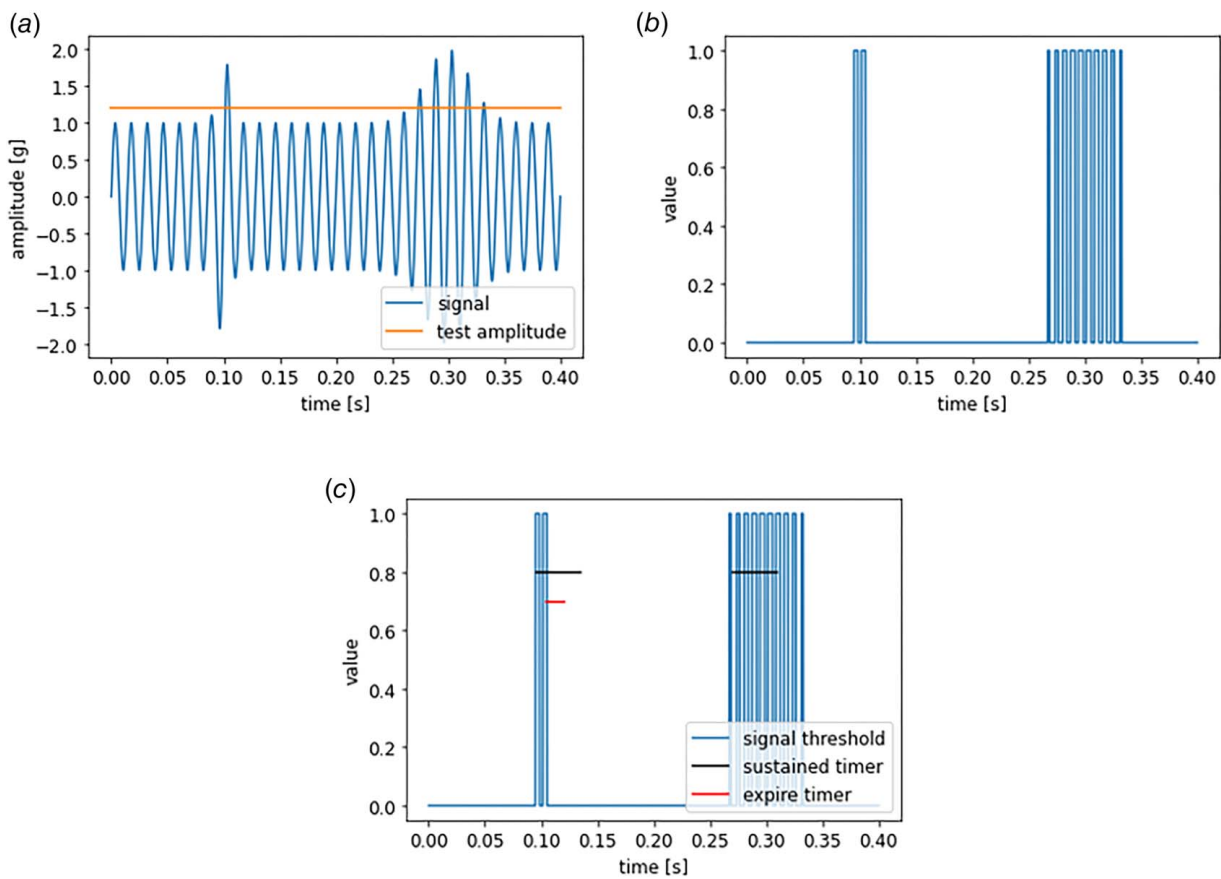


Fig. 8 (a) Test 70 Hz signal with two Gaussian disturbances, (b) the result of the first step of the Expire Timer method applied to the test signal, and (c) an illustration of the two timers used to test the signal

3 Test Methodology

To test the performance of the methods under different sampling rates and noise levels, a simulated signal was used. Testing a simulated signal that was comprised of a sum of cosine waves allowed for the ground truth to be determined. The simulated signal was based on experimental vibration data collected on the outside of a three-axis computer numeric control (CNC) machine.

3.1 Experimental Data. The experimental data were collected on an EMCO E350 three-axis CNC machine. Vibration data were collected using an Analog Devices ADXL203EB-ND

accelerometer. The accelerometer was connected to an MCC118 voltage measurement data acquisition hardware attached on top of a Raspberry Pi 3B+. The purpose of these data was to get a notional idea of the primary spindle harmonics away from the workpiece where a glass scale would be located. The accelerometer placement is shown in Fig. 9(a), and the box used to collect the data from the sensor is shown in Fig. 9(b). The data collection parameters for the sensor and machining process are shown in Table 1.

3.2 Simulated Data. The Fourier transform of the collected vibration data is shown in Fig. 10. In it, there are two dominant harmonics that occur at 6 times and 23 times the tooth pass frequency.

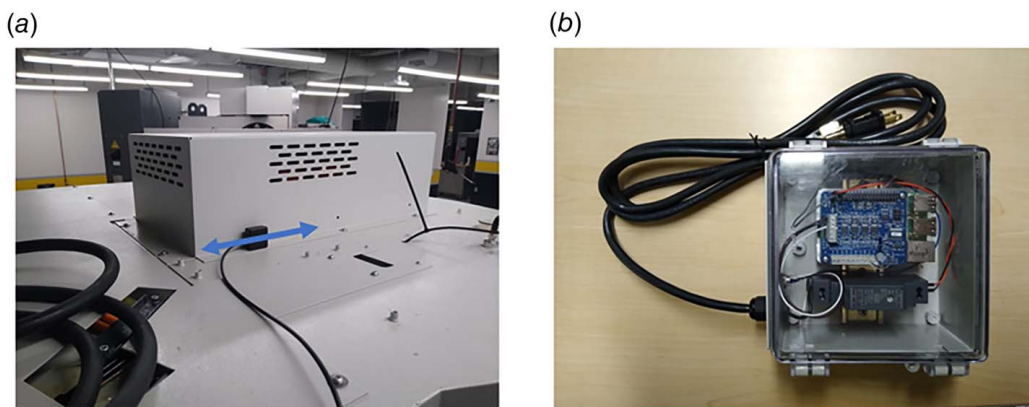
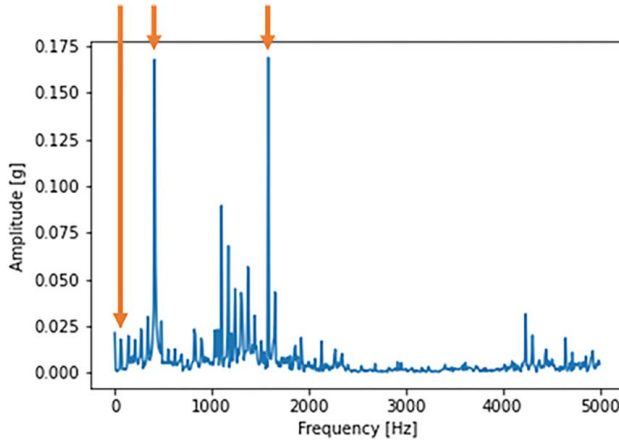


Fig. 9 Experimental setup with (a) accelerometer attached to EMCO where the arrow indicates sensitivity direction and (b) the hardware used to collect the data

Table 1 Experimental data collection parameters

Category	Parameter	Value
Machining	Material	D2 tool steel annealed
	Spindle speed	4220 rpm
	Tool Insert	Kennametal KICR 1/2" single insert
Sensor	Sampling rate	Kennametal SDEB 2615 10,000 Hz

**Fig. 10 Fourier transform of the experimental test data with the tooth pass frequency and the two primary harmonics indicated**

The frequencies of these peaks were used with the tooth pass frequency to create the simulated signal $s(t)$ shown in Eq. (4). The phases (φ_1 and φ_2) assigned to the harmonics are randomly chosen.

$$s(t) = \cos(70 * 2\pi * t) + \cos(6 * 70 * 2\pi * t + \varphi_1) + \cos(23 * 70 * 2\pi * t + \varphi_2) \quad (4)$$

3.3 Signal Disturbances. In addition to stationary signals, the signal processing methods were tested with disturbances modeled after a higher-order Gaussian. The equation for the higher-order Gaussian is given in Eq. (5), where the parameter a is the height,

Table 2 Gaussian parameters for introduced disturbances

Disturbance parameter	Values tested
Power (n)	1, 3
Height (a)	0.5
Standard deviation (σ)	0.005, 0.01

b is the center location, σ is the standard deviation, and n is the power. When n is 1, the equation becomes that of a standard Gaussian [26]. When n is greater than 1, the Gaussian becomes steeper and flatter. The time series for each of the equations was increased by one so the original signal can be multiplied by them, as shown in Eq. (6), to produce the signal with the disturbance.

$$g(t) = 1 + a * e^{-\left(\frac{(t-b)^2}{2 * \sigma^2}\right)^n} \quad (5)$$

$$s(t) = s(t) * g(t) \quad (6)$$

The various values for the Gaussian parameters are given in Table 2. All combinations of these parameters were tested, so in total, four different burst types were tested with the stationary signal for a total of five different base signals. To illustrate each of these, each of the five different disturbances was applied to a stationary signal and shown in Fig. 11.

3.4 Ground Truth. To evaluate the performance of each of the algorithms, the ground truth was extracted from the simulated signals. The maximum sustained amplitude of the simulated signal was the amplitude at which two or more peaks reach or surpass the amplitude and were separated by at least $t_{\text{sustained}}$. The true peaks of the simulated signal were found by setting the first derivative of the signal to zero and solving for values of t in the interval under investigation. Once the peaks were determined, they were sorted and iterated through to find the highest amplitude where the condition above exists.

3.5 Design of Experiment. The values for the sampling rates and signal-to-noise ratios (SNR), calculated as the ratio of the power of the signal to the power of the noise, are summarized in Table 3.

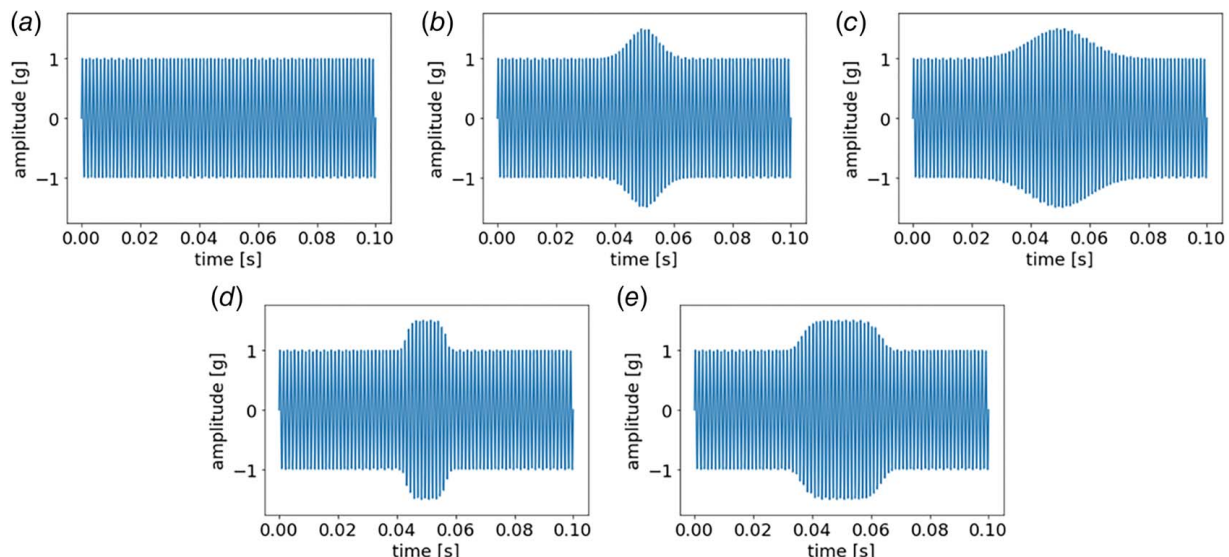
**Fig. 11 Disturbance types applied to a (a) stationary, 800 Hz signal. Disturbances are defined by power, height, and standard deviation as (b) $n=1$, $a=0.5$, $\sigma=0.005$, (c) $n=1$, $a=0.5$, $\sigma=0.01$, (d) $n=3$, $a=0.5$, $\sigma=0.005$, and (e) $n=3$, $a=0.5$, $\sigma=0.01$.**

Table 3 Design of experiment

Parameter	Value
Sampling rate (Hz)	100,000
	10,000
	7500
	5000
SNR	Infinite
	100
	10
	5

The minimum sampling rate (5 kHz) was chosen so that its Nyquist frequency (2.5 kHz) captures the highest frequency component in the simulated signals. The 100 kHz sampling rate was included as an ideal case and was only used when no noise was present. The remaining sampling rates and SNRs are tested by full factorial design, so all possible combinations were tested. This results in 13 test conditions for the nine base signals. For each combination tested, the percentage error of each method relative to the ground truth, as well as the computation time, was recorded. The parameters used to setup the methods are summarized in Table 4.

4 Results

4.1 Stationary Signals. To isolate the variables under test, the effect of the sampling rate and signal-to-noise ratio are considered separately. First, the effect of the sampling rate is investigated by comparing results when no noise is present in the signal. These results are shown in Table 5. Next, the effect of the SNR is considered. The full results are shown in Table 6.

4.2 Non-Stationary Signals. Next, the average performance across the stationary signal and the four test signals with disturbances are considered. The average values are given in Table 7. The standard deviations are reported in Table 8. The average performance across the stationary signal and the four test signals with disturbances are given in Table 9, and the standard deviations are reported in Table 10.

To understand which disturbances are the most difficult to classify, the results of the disturbances are considered. Table 11 presents the error produced by each method with 7.5 kHz sampling rate and no noise. The disturbances are labeled following Fig. 11.

Table 4 Summary of parameters used in each signal processing method

Signal processing method	Parameter	Value
All methods	Sustained time	20 ms
Moving RMS	RMS window width	40 ms
STFT Peaks	Window function	Hann
	Window width	25.6 ms
	Hop size	6.4 ms
	Peak threshold	10% of the highest peak
Peak envelope	Minimum distance between peaks	10 ms
LP rectifier envelope	LPF1 cutoff	10 Hz
	LPF1 order	5
	LPF2 cutoff	200 Hz
	LPF2 order	5
	Replicates	2
Peak distances	No parameters	
Expire timer	Expire timer duration	2 ms
	Replicates	5

Table 5 Percentage error of each method while varying sampling rates on a stationary signal with no noise

	Sampling rate (Hz)			
	100,000	10,000	7500	5000
Moving RMS	-42.1%	-42.1%	-42.1%	-42.1%
STFT peaks	-9.2%	-4.0%	-5.2%	-4.1%
Peak envelope	-1.1%	-2.0%	-2.7%	-6.6%
LP Rectifier envelope	-5.7%	-5.8%	-5.7%	-5.9%
Peak distances	0.0%	0.0%	0.0%	0.0%
Expire timer	-1.9%	-2.1%	-2.5%	-6.4%

Table 6 Percentage error of each method while varying SNR on a stationary signal with a 10 kHz sampling rate

	Signal-to-noise ratio			
	Infinite	100	10	5
Moving RMS	-42.1%	-41.6%	-38.7%	-35.9%
STFT peaks	-4.0%	-1.9%	22.9%	61.4%
Peak envelope	-2.0%	-0.7%	14.4%	21.1%
LP Rectifier envelope	-5.8%	-2.9%	9.4%	18.8%
Peak distances	0.0%	5.5%	25.4%	39.3%
Expire timer	-2.1%	2.3%	13.2%	21.7%

Table 7 Average percentage error of each method across multiple disturbance types while varying sampling rates with no noise

Method	Sampling rate (Hz)			
	100,000	10,000	7500	5000
Moving RMS	-43.0%	-43.0%	-43.1%	-43.1%
STFT peaks	-0.6%	5.4%	5.5%	5.3%
Peak envelope	3.7%	2.2%	1.6%	-2.6%
LP Rectifier envelope	-1.1%	-1.1%	-1.1%	-1.0%
Peak distances	0.0%	-0.3%	-0.3%	-3.2%
Expire timer	-0.5%	-0.9%	-1.0%	-7.1%

Table 8 Standard deviation of each method across multiple disturbance types while varying sampling rates with no noise

Method	Sampling rate (Hz)			
	100,000	10,000	7500	5000
Moving RMS	0.039	0.039	0.038	0.038
STFT peaks	0.078	0.055	0.062	0.055
Peak envelope	0.058	0.064	0.067	0.065
LP Rectifier envelope	0.071	0.072	0.071	0.069
Peak distances	0.000	0.003	0.003	0.044
Expire timer	0.008	0.007	0.009	0.022

Table 9 Average percentage error of each method across multiple disturbance types while varying SNR

Method	Signal-to-noise ratio			
	Infinite	100	10	5
Moving RMS	-43.0%	-42.6%	-41.9%	-39.2%
STFT peaks	5.4%	5.9%	27.3%	61.2%
Peak envelope	2.2%	3.9%	15.2%	20.1%
LP rectifier envelope	-1.1%	1.0%	11.3%	19.2%
Peak distances	-0.3%	5.7%	21.3%	32.0%
Expire timer	-0.9%	4.7%	15.9%	22.3%

Table 12 presents the error produced by each method with 7.5 kHz sampling rate and an SNR of 10.

4.3 Computation Time. The computation time of each method was averaged over 1000 executions. This was repeated three times and the best result is reported in Table 13. This process was repeated for two sampling rates, 10,000 Hz and

Table 10 Standard deviation of each method across multiple disturbance types while varying SNR with a 10 kHz sampling rate

Method	Signal-to-noise ratio			
	Infinite	100	10	5
Moving RMS	0.039	0.039	0.050	0.053
STFT peaks	0.049	0.045	0.062	0.060
Peak envelope	0.062	0.036	0.026	0.076
LP rectifier envelope	0.072	0.063	0.037	0.028
Peak distances	0.003	0.005	0.060	0.100
Expire timer	0.007	0.014	0.031	0.035

Table 11 Error in the presence of different disturbances with a 7.5 kHz sampling rate and no noise

	Disturbance				
	a	b	c	d	e
Moving RMS	-42.1%	-41.8%	-49.8%	-41.2%	-40.5%
STFT Peaks	-5.2%	10.6%	5.9%	7.6%	8.5%
Peak envelope	-2.7%	-3.8%	6.4%	-2.7%	11.2%
LP rectifier	-5.7%	-6.7%	3.4%	-5.7%	9.4%
Envelope					
Peak distances	0.0%	-0.6%	-0.5%	0.0%	-0.5%
Expire timer	-2.5%	-0.7%	-0.6%	-0.7%	-0.5%
RMS (excluding Moving RMS)	3.4%	4.6%	4.5%	4.5%	7.9%

Table 12 Error in the presence of different disturbances with a 7.5 kHz sampling rate and an SNR of 10

	Disturbance				
	a	b	c	d	e
Moving RMS	-39.3%	-38.9%	-37.4%	-38.2%	-36.6%
STFT peaks	31.5%	45.8%	33.5%	47.2%	37.3%
Peak envelope	2.1%	1.0%	-14.2%	2.1%	-14.5%
LP rectifier Envelope	1.5%	0.5%	3.1%	1.5%	3.1%
Peak distances	23.4%	22.7%	8.5%	24.0%	14.7%
Expire timer	2.7%	5.3%	8.0%	2.8%	14.5%
RMS (excluding Moving RMS)	18.1%	22.8%	14.4%	20.4%	20.6%

Table 13 Timing results for each of the signal processing methods in milliseconds

Method	Samples		
	1000	10,000	Ratio
Moving RMS	0.19 ms	0.67 ms	3.5
STFT peaks	2.27	9.96	4.4
Peak envelope	0.44	1.46	3.4
LP Rectifier envelope	98.7	812	8.2
Peak distances	0.13	0.33	2.5
Expire timer	2.52	25.1	9.9

Table 14 Minimum detectable frequencies for the tuning parameters used in this work

Signal processing method	Minimum detectable frequency (Hz)
Moving RMS	50
STFT peaks	39
Expire timer	50

100,000 Hz. A 0.1 s signal was analyzed so the methods were executed on 1000 and 10,000 samples. This was done to give an indication of how the time to execute the method scales with sampling rate. These results were produced on a laptop with an eighth-generation Intel i5 chip.

5 Discussion

From the large amount of error of the *Moving RMS* method across all test cases, it is clear that the relationship between the RMS and the peaks in a single sine wave does not hold for a signal that is comprised of a base frequency and harmonics of it. This is because the relationship of the RMS value and the peak value changes depending on the number of sine waves comprising the signal. This could be corrected for in the test signal with three sine waves, but the result could not be applied generally to other signals. For this reason, discussion of the *Moving RMS* method is largely omitted from the remainder of this section.

5.1 Stationary Signals. When it came to the performance on a stationary signal, the sampling rate was found to have the greatest effect on the *Expire Timer* and *Peak Envelope*. For these two methods, reducing the sampling rate led to underestimations. This is expected, as reducing the sampling rate makes it more likely for peaks to be missed. The other methods were less sensitive to changes in the sampling rate. When evaluating the effect of noise, the *STFT Peaks* method was found to have the greatest sensitivity followed by the *Peak Distances* method. The effect was reduced on the other methods, but all methods saw that increasing the noise in the signal led to overestimations. This is expected since noise increases the amplitude of the input signal. The presence of noise adds peaks to the Fourier transform, so it was expected that the *STFT Peaks* method would lead to larger amounts of error in the presence of noise.

5.2 Non-Stationary Signals. After disturbances were added to the signals, the *LP Rectifier Envelope* was found to have the largest range in performance across all sampling rates. It was also seen that the *STFT Peaks* had the greatest amount of error, and the *Expire Timer* had the greatest decrease in performance as the sampling rate was reduced. With the sampling rate constant and varying SNR, the performance of all methods followed similar trends to when disturbances were not present. When looking at the performance on the 7.5 kHz signal without noise, the effect of the disturbance was seen to be minimal. Disturbance e, which has the sharpest rise and wide plateau, had the highest error on average. This is expected, since the sharp rise and fall are more difficult to envelope, and the envelope methods had greater error than the non-envelope methods. When looking at the effect of the disturbances on the 7.5 kHz signal with an SNR of 10, no disturbance case was significantly worse than the others, and case c performed better than the average. The addition of noise helps reduce the effect of the steep rise so case e is no longer the worst case. This additional noise also increases the predicted output of case c, which was initially underestimated, ultimately making it more accurate.

5.3 Computation Time. In the timing experiment, it was seen that when the methods were fed 1000 samples representing 100 ms of data, all the methods were able to complete the computation

Table 15 Summary of the performance across all test cases

	Stationary				Non-stationary					Time
	Sampling rate (kHz)	SNR			Sampling rate (kHz)	SNR				
Method	5	10	10	100	5	10	10	100	—	+
Moving RMS	—	—	—	—	—	—	—	—	—	+
STFT peaks	+	+	—	+	o	o	—	o	o	+
Peak envelope	+	+	o	+	—	—	—	o	o	+
LP rectifier envelope	+	+	o	+	—	—	—	—	—	o
Peak distances	+	+	—	+	o	+	—	+	+	+
Expire timer	+	+	o	+	o	+	—	+	+	+

Key: +: lerror < 7% and $\sigma < 3\%$; o: lerror < 15% and $\sigma < 6\%$; -: lerror > 15% and $\sigma > 6\%$.

within 100 ms, allowing it to fully complete before a new batch of data becomes available when processing in real-time. The *LP Rectifier Envelope*, however, barely met this requirement and failed to process 10,000 samples representing 100 ms of data sampled at 100 kHz. For this reason, if processing data in real-time, a method other than the *LP Rectifier Envelope* should be considered.

In the development of the *Moving RMS*, *STFT Peaks*, and *Expire Timer* methods, there is a mathematical basis for a minimum detectable frequency that the methods will not be expected to perform reliably below. This is important to consider if they are being applied to a broadband signal, where low frequencies are expected. In this work, the parameters used lead to the minimum detectable frequencies shown in Table 14.

5.5 Summary. A summary of the performance of each method across all the test conditions is given in Table 15; this table gives a granular view of how each method generally performs. For the stationary test cases, the methods are evaluated by the magnitude of the error they produce. Error less than 5% is considered acceptable. Between 5% and 10% is considered borderline, and above 10% is unacceptable. For the non-stationary test cases, the standard deviation is also considered. Standard deviations below 3% or above 6% are considered unacceptable. This high-level summary indicates that the *Peak Envelope* generally produces the least error. The *Peak Envelope* method, however, had the most error at low sampling rates in stationary signals, so if this is the kind of signal that is expected, other methods should be considered.

6 Conclusion

This work developed and tested methods for the extraction of sustained amplitudes from vibration data. Six methods were formalized in two categories: envelope and non-envelope. A simulated signal was used to evaluate the performance of each of these methods under various sampling rates, noise levels, and disturbances. The results of these tests inform users on how to process vibration signals to determine the sustained amplitudes, and what the limitations of each method are. Additionally, with one exception, all methods can be used in real-time. This is valuable in a manufacturing application because optical encoders, which are sensitive to sustained vibrations, are used to determine the location of CNC and coordinate measuring machines. Monitoring their vibration levels allows operators to be informed about the vibration levels and realize when errors may be introduced.

Acknowledgment

This work was supported by the U.S. Department of Energy (DOE) DE-EE0008303 and the U.S. Department of Defense (DOD), Office of Local Defense Community Cooperation (OLDCC), Industry Resilience Program, Award #ST1449-21-03 2016-2166.

Conflict of Interest

There are no conflicts of interest.

Data Availability Statement

The datasets generated and supporting the findings of this article are obtainable from the corresponding author upon reasonable request.

References

- Takata, S., Kirnura, F., van Houten, F., Westkamper, E., Shpitalni, M., Ceglarek, D., and Lee, J., 2004, "Maintenance: Changing Role in Life Cycle Management," *CIRP Ann.*, **53**(2), pp. 643–655.
- Atzori, L., Iera, A., and Morabito, G., 2010, "The Internet of Things: A Survey," *Comput. Netw.*, **54**(15), pp. 2787–2805.
- Jeschke, S., Brecher, C., Meisen, T., Özdemir, D., and Eschert, T., 2017, "Industrial Internet of Things and Cyber Manufacturing Systems," *Industrial Internet of Things*, S. Jeschke, C. Brecher, H. Song, and D. Rawat, eds., Springer, Cham, pp. 3–19.
- Lee, J., Bagheri, B., and Jin, C., 2016, "Introduction to Cyber Manufacturing," *Manuf. Lett.*, **8**(1), pp. 11–15.
- Randall, R. B., 2011, *Vibration-Based Condition Monitoring: Industrial, Aerospace and Automotive Applications*, John Wiley & Sons, Hoboken, NJ.
- Colledani, M., Tolio, T., Fischer, A., Iung, B., Lanza, G., Schmitt, R., and Vánčza, J., 2014, "Design and Management of Manufacturing Systems for Production Quality," *CIRP Ann.*, **63**(2), pp. 773–796.
- Oiwa, T., and Katakui, M., 2015, "Survey of Questionnaire on Ultra-Precision Positioning," *J. Jpn. Soc. Precis. Eng.*, **81**(10), pp. 904–910.
- Gao, W., Kim, S., Bosse, H., Haitjema, H., Chen, Y., Lu, X., Knapp, W., Weckemann, A., Estler, W., and Kunzmann, H., 2015, "Measurement Technologies for Precision Positioning," *CIRP Ann.*, **64**(2), pp. 773–796.
- Alejandre, I., and Artes, M., 2004, "Machine Tool Errors Caused by Optical Linear Encoders," *Proc. Inst. Mech. Eng. B*, **218**(1), pp. 113–122.
- Lopez, J., and Artes, M., 2012, "A New Methodology for Vibration Error Compensation of Optical Encoders," *Sensors*, **12**(4), pp. 4918–4933.
- Lopez, J., Artes, M., and Alejandre, I., 2011, "Analysis of Optical Linear Encoders' Errors Under Vibration at Different Mounting Conditions," *Measurement*, **44**(8), pp. 1367–1380.
- Vlachos, M., Wu, K.-L., Chen, S.-K., and Yu, P., 2005, "Fast Burst Correlation of Financial Data," European Conference on Principles of Data Mining and Knowledge Discovery, Porto, Portugal, Oct. 3–7.
- Friis-Christensen, E., and Lassen, K., 1991, "Length of the Solar Cycle: An Indicator of Solar Activity Closely Associated With Climate," *Science*, **254**(5032), pp. 698–700.
- Leland, W., Taqqu, M., Willinger, W., and Wilson, D., 1994, "On the Self-Similar Nature of Ethernet Traffic (Extended Version)," *IEEE/ACM Trans. Netw.*, **2**(1), pp. 1–15.
- Widdowson, M.-A., Bosman, A., Stratton, E. V., Tinga, M., Chaves, S., Eerden, L. V., and Pelt, W. V., 2003, "Automated, Laboratory-Based System Using the Internet for Disease Outbreak Detection, The Netherlands," *Emerg. Infect. Dis.*, **9**(9), pp. 1046–1052.
- Leskovec, J., Backstrom, L., and Kleinberg, J., 2009, "Meme-Tracking and the Dynamics of the News Cycle," Proceedings of the 15th ACM SIGKDD International Conference on Knowledge Discovery and Data Mining, Paris, France, June 28–July 1.
- Zhu, Y., and Shasha, D., 2003, "Efficient Elastic Burst Detection in Data Streams," Proceedings of the Ninth ACM SIGKDD International Conference on Knowledge Discovery and Data Mining, Washington, DC, Aug. 24–27.
- Legendy, C., and Salcman, M., 1985, "Bursts and Recurrences of Bursts in the Spike Trains of Spontaneously Active Striate Cortex Neurons," *J. Neurophysiol.*, **53**(4), pp. 926–939.
- Kleinberg, J., 2003, "Bursty and Hierarchical Structure in Streams," *Data Min. Knowl. Discov.*, **7**(4), pp. 373–397.

[20] Polycarpou, A., Soom, A., Swarnakar, V., Valtin, R., Acharya, R., Demjanenko, V., Soumekh, M., Beneson, D., and Porter, J., 1996, "Event Timing and Shape Analysis of Vibration Bursts From Power Circuit Breakers," *IEEE Trans. Power Deliv.*, **11**(2), pp. 848–857.

[21] Zhou, N., and Dagle, J., 2014, "Initial Results in Using a Self-Coherence Method for Detecting Sustained Oscillations," *IEEE Trans. Power Syst.*, **30**(1), pp. 522–530.

[22] Müller, M., 2015, "Fourier Analysis of Signals," *Fundamentals of Music Processing: Audio, Analysis, Algorithms, Applications*, Springer, Cham, pp. 39–114.

[23] Huang, N., Shen, Z., Long, S., Wu, M., Shih, H., Zheng, Q., Yen, N.-C., Tung, C., and Liu, H., 1998, "The Empirical Mode Decomposition and the Hilbert Spectrum for Nonlinear and Non-Stationary Time Series Analysis," *Proc. R. Soc. A: Math. Phys. Eng. Sci.*, **454**(1971), pp. 903–995.

[24] Virtanen, P., Gommers, R., Oliphant, T. E., Haberland, M., Reddy, T., Cournapeau, D., Burovski, E., et al., 2020, "SciPy 1.0: Fundamental Algorithms for Scientific Computing in Python," *Nat. Methods*, **17**(3), pp. 261–272.

[25] Jeong, J., Kimball, D., Kwak, M., Hsia, C., Draxler, P., and Asbeck, P., 2009, "Wideband Envelope Tracking Power Amplifiers With Reduced Bandwidth Power Supply Waveforms and Adaptive Digital Predistortion Techniques," *IEEE Trans. Microw. Theory Tech.*, **57**(12), pp. 3307–3314.

[26] Parent, A., Morin, M., and Lavigne, P., 1992, "Propagation of Super-Gaussian Field Distributions," *Opt. Quantum Electron.*, **24**(9), pp. S1071–S1079.